

Rational design of systematic AIEEgens further modified by substituents from a novel chain structure

Hao Lu¹, Kun Wang², Beibei Liu¹, Meng Wang¹, Mingming Huang¹, Yue Zhang¹ & Jiping Yang^{1*}

¹Key Laboratory of Aerospace Advanced Materials and Performance, Ministry of Education, School of Materials Science and Engineering, Beihang University, Beijing 100191, China;

²State Key Laboratory of Advanced Power Transmission Technology, State Grid Global Energy Interconnection Research Institute, Beijing 102211, China

Received June 2, 2020; accepted July 16, 2020; published online September 15, 2020

The expansion of new structures in aggregation-induced emission/aggregation-induced emission enhancement (AIE/AIEE) systems has attracted persistent attention recently, from which more luminescent functional molecules with characteristic skeletons are derived to satisfy specialized applications. In this study, a series of derivatives cored by tetraphenyl enamine with various terminal groups were designed and synthesized based on a novel p- π conjugate chain structure ($-\text{C}=\text{C}-\text{N}-$). Experimental and theoretical studies reveal that attaching modified groups to enamine core is decisive to achieve successful conversion from non-luminescence to AIEE-activity. Moreover, due to different substituent effect on electronic structure, molecular conformation and molecular packing, diverse enamine compounds exhibited prominent substituent tunable emission properties, realizing regulated AIEE effect and multicolor emitting. These results not only offer a new method to design AIEgens/AIEEgens with p- π conjugate chain structures, but also provide in-depth knowledge for functional modifications of more novel AIE/AIEE units and materials.

aggregation-induced emission enhancement, chain structure, enamine derivatives, substituent tunable emission

Citation: Lu H, Wang K, Liu B, Wang M, Huang M, Zhang Y, Yang J. Rational design of systematic AIEEgens further modified by substituents from a novel chain structure. *Sci China Chem*, 2020, 63, <https://doi.org/10.1007/s11426-020-9831-y>

1 Introduction

Aggregation-induced emission/aggregation-induced emission enhancement luminogens (AIEgens/AIEEgens), initially proposed and investigated by Tang *et al.* in 2001, are of great significance due to their wide applications in chemosensors, bio-imaging, optoelectronics [1–9], *etc.* So far, hundreds of compounds have been exploited to exhibit AIE/AIEE properties. Based on the primary characteristic of molecular structures, they can be divided into the following categories as pure hydrocarbon aromatics, organic heteroa-

tom molecules and clusterization-triggered luminophores [10–12]. Among these types of AIEgens/AIEEgens, organic luminescent molecules with conjugate chain structures are regarded as a crucial constitution. Generally, most AIE/AIEE luminogens feature propeller-like configuration with several rotors attaching to a stator, which are obedient to the most accepted AIE/AIEE mechanism, namely as the restriction of intramolecular motion (RIM) [13–15]. From this point of view, conjugate chains should be a benign candidate of stator structures, and a series of phenyl-substituted AIE/AIEE systems owning conjugate chains have been reported, such as tetraphenylethenes, tetrathienylethenes, distyrylanthracene [16–18].

*Corresponding author (email: jyang@buaa.edu.cn)

3 Results and discussion

3.1 Photo-physical properties

Firstly, the spectral tests in dilute solution were used to investigate optical properties of these synthesized enamine derivatives. Their absorption behaviors and normalized emission spectra in THF solution (10^{-4} M) are shown in Figure 2. The basic spectroscopic parameters are summarized in Table S1 (Supporting Information online).

As shown in Figure 2(a), the compounds with diverse modifications (bromine, hydroxyl, methoxyl, double methoxyls and nitro) severally showed different absorption bands with peaks at 319, 304/321, 303/319, 311/336 and 310/410 nm. Also, these enamine derivatives (Br-B1-A1, HO-B1-A1, MeO-B1-A1, MeO-B1-A1-OMe and NO₂-B1-A1) all showed strong absorption capability with molar extinction coefficients of 23,626, 27,154, 24,173, 25,014 and 17,900 L mol⁻¹ cm⁻¹, respectively. The absorption at approximately 310 nm of all substances was typical conjugate transition of the enamine structure, which corresponded to the absorption wavelength calculated by the transition energy of initial B1-A1 structure (Figure S8). Meanwhile, some shoulder absorptions appeared at the range from 340 to 370 nm for Br-B1-A1, HO-B1-A1, MeO-B1-A1 and MeO-B1-A1-OMe. Unlike the compounds with moderate terminal groups, the introduction of strong electron-withdrawing nitro group greatly changed the absorption feature of corresponding neutral enamine compound, and a sharp long-wavelength absorption peak appeared at 410 nm. Valuably, the bathochromic-shift degree for all enamine derivatives was consistent with the electron-donating capacities of their diverse modifications, implying that the main cause of long-wavelength absorption should be the intramolecular charge transfer (ICT) effect from the relatively electron-rich moiety to the electron-deficient part [34]. Represented by NO₂-B1-A1, the UV absorption spectra in different mixtures of *n*-hexane and chloroform demonstrated the long-wavelength absorptions gradually redshifted accompanying with the increased solvent polarity (Figure S9), further verifying the ICT feature of long-wavelength absorptions.

Furthermore, the emission spectra of these enamine deri-

vatives were recorded in THF (10^{-4} M), as illustrated in Figure 2(b). With a view to the transition of local excited state, all compounds unfolded emission peaks at approximately 430 nm apart from NO₂-B1-A1. At the same time, some emission shoulders or peaks appeared at about 460 nm for Br-B1-A1, 500 nm for HO-B1-A1, 510 nm for MeO-B1-A1, and 540 nm for MeO-B1-A1-OMe. Moreover, it was revealed that corresponding wavelengths of these shoulders and peaks were dependent on the electronic-donating abilities of diverse modifications. These results mean that the peaks may be caused by the transition of twisted intramolecular charge transfer (TICT) excited state [35], indicating the possibility to achieve tunable emission by changing the terminal substituent groups. For NO₂-B1-A1, owing to the existence of conspicuous D-A structure, its PL emission peak was at around 620 nm with a large Stokes shift ($\Delta\lambda > 180$ nm).

3.2 Aggregation-induced emission enhancement characteristics

The AIE/AIEE properties of enamine derivatives were then explored. The different amounts of water, a poor solvent for these luminogens, were added to the pure THF solutions by adjusting the water fractions between 0 and 95%, and the emission changes were further monitored through PL spectra.

As shown in Figure 3(a), for MeO-B1-A1, when the water content was less than 70%, slight emission enhancement occurred. Nevertheless, after the content of water exceeded 70%, the luminous intensity significantly raised. Ultimately, the luminous intensity of MeO-B1-A1 solution containing 95% water had 90-fold increase in comparison to its pure THF solution, showing typical AIEE characteristic [36]. In the inset of Figure 3(a), the fluorescent image also visually exhibited the tremendous change of MeO-B1-A1 solutions in THF/water mixtures containing 0 and 95% water. Usually, the mutation point is closely related to the formation of nano-aggregates, demonstrating coincident correlation between aggregating state and fluorescence intensity in the MeO-B1-A1 system [37]. The PL intensity hardly changed before the

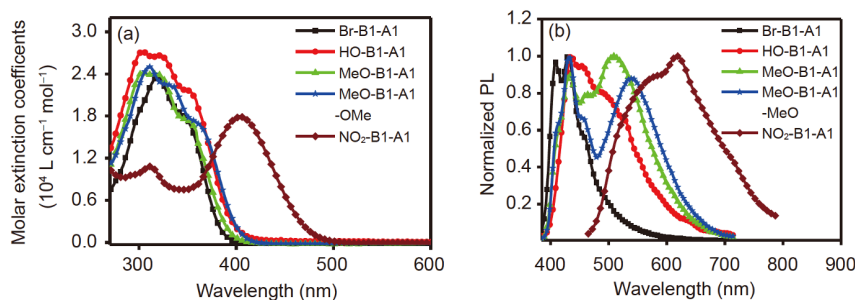


Figure 2 Absorption behaviors (a) and normalized emission (b) spectra of five enamine derivatives in THF (concentration: 10^{-4} M; excitation wavelengths: 365 nm for Br-B1-A1, HO-B1-A1, MeO-B1-A1 and MeO-B1-A1-OMe, 410 nm for NO₂-B1-A1; EX slit: 5 nm; EM slit: 10 nm) (color online).

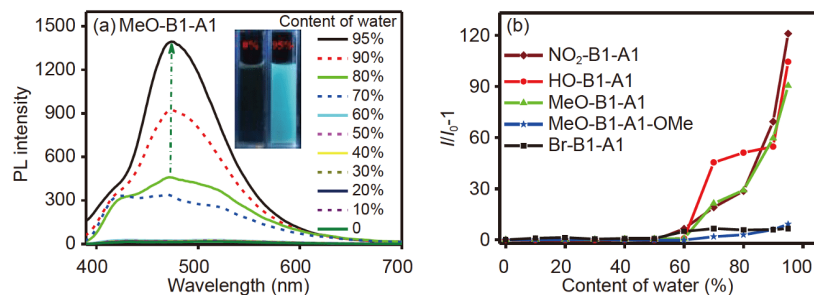


Figure 3 (a) Emission spectra of MeO-B1-A1 in THF/water mixtures under excitation at 365 nm (10^{-3} M; EX slit: 5 nm; EM slit: 10 nm). Inset: fluorescent images of MeO-B1-A1 in THF/water mixtures containing 0 and 95% water. (b) Plots of $(I/I_0)-1$ vs. water content for five enamine derivatives, where I_0 is the luminescence intensity in pure THF (color online).

water content reached 70% as no obvious aggregation appeared. In contrast, evident aggregation occurred while the content of water was over 70%, resulting in a rapid increase of emission intensity. Represented by MeO-B1-A1, the aggregation was convincingly demonstrated by the Mie effect in the UV absorption curves at various proportions of THF and water (Figure S10) [38]. In the meantime, accompanying with enhanced water fraction, the long-wavelength emission gradually disappeared, and a novel emission peak aroused at 475 nm when water content reached to 95%. In comparison to the dilute solution state, whose emission peak position located at around 430 nm, the molecular structure of MeO-B1-A1 became more planar due to the crowded space in aggregation state, contributing to the bathochromic shift emission.

Similar to the PL performance of MeO-B1-A1, other enamine derivatives all presented typical AIEE behaviors, which were displayed in Figure S11. Their turning point values of fluorescence intensity all focused on 60% or 70%, which were consistent with their analogous molecular size. Moreover, there were still some other similarities and differences to be elucidated detailly. In the mixed solutions containing 95 vol% water, the fluorescence wavelength of Br-B1-A1, HO-B1-A1, MeO-B1-A1-OMe and NO_2 -B1-A1 was at 414, 471, 508 and 590 nm, respectively. Besides the fluorescence wavelength, the AIEE behavior of HO-B1-A1 was parallel to MeO-B1-A1 with 104-fold increase of luminous intensity. That means the terminal hydroxyl and methoxy exhibit similar substituent influence on the emission performance of original enamine molecule. For Br-B1-A1, the PL spectra showed multiple peaks or shoulders due to the weak auxochrome property and heavy atom effect of bromine substitution [39], and the luminous intensity increased by only seven times at the 95% water volume fraction. With respect to MeO-B1-A1-OMe, although the introduction of double methoxyls afforded more freedom space for energy consumption, the enhanced auxochrome effect was beneficial for stronger emission. Thus, MeO-B1-A1-OMe also indicated relatively small enhancement (9-fold) in the 95 vol% water solution. When regarding to

NO_2 -B1-A1, its PL intensity exhibited a huge 121-fold promotion from 0% to 95 vol% water solution in AIEE test. This phenomenon is opposite to common cognizance, as nitrophenyl group is usually considered as a famous electron and energy acceptor and acted as a fluorescence quencher. The reason may be that the single nitro is still not adequate to overpower the AIE/AIEE effect [40], and the substituent effect of nitro has greatly changed the aggregation emission ability of original B1-A1 structure (illustrated in the following analysis). This phenomenon is attracting and further research of the corresponding cause and application is still underway.

Generally, the AIEE behaviors of five enamine derivatives are summarized in Figure 3(b). As we have reported before [33], the fluorescence quantum efficiency of B1-A1 was just 0.01% and 0.02% in THF solution state and solid powder state, respectively, exhibiting non-luminous characteristic. In comparison to the original non-emissive B1-A1 molecule, all modified enamines brought out AIEE-active properties. Comparing to their fluorescence intensities in dilute solutions and in 95 vol% water systems, the fluorescence intensities of Br-B1-A1 and MeO-B1-A1-OMe increased by 10 times, and those of HO-B1-A1, MeO-B1-A1 and NO_2 -B1-A1 promoted by 100 times. The results of quantum yield in both solution and solid states of these enamines further proved these investigations, which are presented in Table S2. Their quantum yields were remarkably higher in the powder state contrast to in the solution state. In addition, the increased ratios of the quantum yield data are consistent with these of fluorescence intensity in AIEE experiments for the derivatives. Combining the aforesaid results, it is concluded that successful conversion can be achieved from non-luminance to AIEE-activity through suitable modifications based on the tetraphenyl enamine structure with p- π conjugate chain skeleton. Furthermore, the results reveal the notable substituent effect on the optical properties and AIEE performance of these enamine derivatives, providing valuable guidance for the modification of undesirable non-emissive compounds with heteroatom conjugate chains.

3.3 Substituent tunable emission properties

As mentioned above, all derivatives are based on the skeleton of tetraphenyl enamine and only differ in the type or number of modified groups. So, to investigate the substituent influence on optical properties of these enamines deeply, their pivotal photo-physical parameters and solid emission behaviors were further researched.

As we all know, the photoluminescent behavior of a molecule is mainly determined by radiative and nonradiative decay in excited state. The corresponding rates (k_r and k_{nr}) are represented in the following two formulas [41]:

$$\phi_F = k_r / (k_r + k_{nr}) \quad (1)$$

$$\tau = 1 / (k_r + k_{nr}) \quad (2)$$

In the statement, ϕ_F is the quantum yield and τ refers to the average fluorescence lifetime. All enamines' fluorescence lifetimes were measured in both dilute THF solution and solid powder states, which were shown in Figure S12 and further summarized in Table 1. In detail, their PL lifetime values were gained as 4.04, 2.42, 4.06, 9.13, 0.16 ns in dilute solutions and 4.30, 4.61, 8.73, 23.55, 0.48 ns in solid powder states for Br-B1-A1, HO-B1-A1, MeO-B1-A1, MeO-B1-A1-OMe and NO₂-B1-A1, respectively. Assuredly, these results reveal that terminal modifications have remarkable effect on their fluorescence lifetimes. The strong electron-absorbing group (–NO₂) attenuates the fluorescence lifetime drastically, yet the introduction of auxochromes is conducive to enhance the fluorescence lifetime of these derivatives. It is worth mentioning that the fluorescence lifetime of MeO-B1-A1-OMe in powder state was determined to be 23.55 ns, which is rather long for an organic fluorescent molecule [42].

Furthermore, from dilute THF solution state to solid powder state, the k_r values all increased tremendously for HO-B1-A1, MeO-B1-A1 and NO₂-B1-A1, accompanying with distinctly decline of their k_{nr} values. These results are beneficial to typical AIEE properties and coincident with their roughly 100-fold fluorescence enhancement. With respect to Br-B1-A1, its k_r improved a lot whereas the k_{nr} decreased rarely from dilute solution to solid powder state, thus resulting in a relatively smaller increase in emission intensity. Moreover, in pure THF solution, the obviously

higher ϕ_F of MeO-B1-A1-OMe is deduced to be stemmed from its larger k_r and smaller k_{nr} , and the major cause may be manifested as the better conjugated molecular structure of double methoxyl modification [43]. Dissimilarly, in solid powder state, the k_r kept almost constant and the k_{nr} was down by half. These consequences mean that the main cause of AIEE performance is just dependent by effecting the nonradiative decay channel in the aggregating condition, therefore the emission enhancement of MeO-B1-A1-OMe is relatively small.

Not only the AIEE behaviors of the compounds, but also the emission wavelengths were found to be influenced by the side groups. As mentioned above, various enamines exhibited different emission wavelengths in the 95 vol% water systems. To gain insight into the distinction of emitting colors affected by modifications, the emission behaviors of Br-B1-A1, HO-B1-A1, MeO-B1-A1, MeO-B1-A1-OMe and NO₂-B1-A1 in the solid powder state were also tested, indicating maximum emission wavelengths at 449, 483, 483, 518 and 624 nm, respectively (Figure 4(a)). Comparing to the solution state, the emission wavelengths of whole enamine compounds indicated apparent redshift in the powder state. Actually, well-organized and flatter conformations may produce along with the increased degree of aggregation, consequently leading to the redshift of emission peaks. In addition, the CIE1931 diagrams and chromaticity coordinates of these powder samples were also illustrated in Figure 4(b), among which the emission colors of Br-B1-A1, HO-B1-A1, MeO-B1-A1, MeO-B1-A1-OMe and NO₂-B1-A1 were blue, cyan, cyan, green and red with the chromaticity coordinates represented as (0.16, 0.13), (0.15, 0.32), (0.16, 0.33), (0.24, 0.41), and (0.61, 0.35), respectively. Thus, by analyzing the fluorescent performance of enamine derivatives with different terminal modifications in the 95 vol% water solution, solid powder state and CIE coordinate, it is concluded that different modification strategies have noteworthy influence on luminescence color, showing meaningfully substituent tunable characteristics. These results enlighten that the diverse emitting colors of enamines can be realized by modification strategies, providing guidance for the design of colorful p- π conjugate chain compounds.

Table 1 Average fluorescence lifetimes and radiative and nonradiative decay rates for five enamine compounds

| | $\langle\tau\rangle$ (ns) | | $k_r^{(c)}$ ($\times 10^6$ s ⁻¹) | | $k_{nr}^{(c)}$ ($\times 10^8$ s ⁻¹) | |
|------------------------|---------------------------|---------------------|---|-------|--|-------|
| | Soln ^{a)} | Solid ^{b)} | Soln | Solid | Soln | Solid |
| Br-B1-A1 | 4.04 | 4.30 | 0.0495 | 0.372 | 2.48 | 2.33 |
| HO-B1-A1 | 2.42 | 4.61 | 0.0826 | 2.60 | 4.13 | 2.14 |
| MeO-B1-A1 | 4.06 | 8.73 | 0.148 | 1.27 | 2.46 | 1.13 |
| MeO-B1-A1-OMe | 9.13 | 23.55 | 0.110 | 0.110 | 1.10 | 0.42 |
| NO ₂ -B1-A1 | 0.16 | 0.48 | 3.13 | 227 | 62.50 | 18.60 |

a) In THF solution (10⁻⁴ M). b) Solid powder. c) The radiative decay rate $k_r = \phi_F / \tau$; the nonradiative decay rate $k_{nr} = 1 / \tau - k_r$.

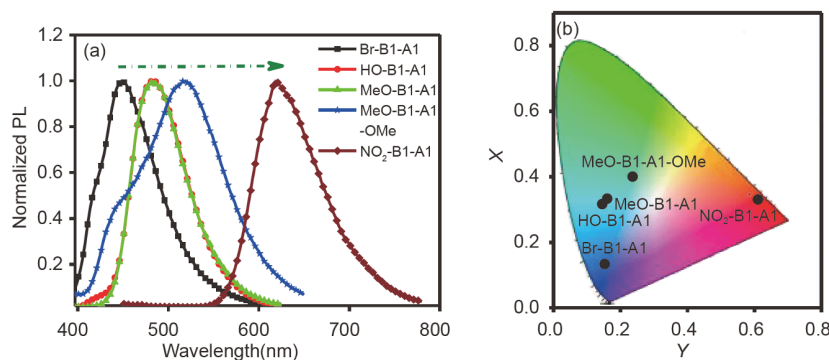


Figure 4 (a) Normalized emission spectra of all five enamine derivatives in solid powder states (excitation wavelengths: 365 nm; EX slit: 2.5 nm; EM slit: 2.5 nm). (b) CIE1931 diagram and the chromaticity coordinates of the solid enamine samples (color online).

To summarize, from elementary tetraphenyl enamine structure to multiple derivatives with various modifications, the key role of substituents has been confirmed in the aforementioned statements. However, the related mechanisms are still unclear as following: (1) How is the AIEE effect of modified enamines realized? (2) What are the reasons of different AIEE behaviors about modified enamines with different terminal groups? (3) What are the causes of tunable optical physical properties of diverse enamines? These issues need further research and discussions.

3.4 Electronic and geometric structures

In order to gain insight into the above questions, theoretical calculation was conducted to make further analysis. At first, the nature of nonluminous performance on B1-A1 molecule should be understood. Theoretical simulation of B1-A1 was based on the (TD) B3LYP/6-31G(d) level in THF and modeled by PCM and ONIOM approaches in the crystal state [44]. Computational results showed that the oscillator strengths (f) in $S_1 \rightarrow S_0$ transition of B1-A1 were gained as 0.04 and 0.20 in the solution and the crystal state, in which the transition between the LUMO and HOMO (LUMO=lowest unoccupied molecular orbital, HOMO=highest occupied molecular orbital) accounted for 99% and 98%, correspondingly (Figure S13). On the basis of the consequences, B1-A1 should own certain luminescent capability in solid state theoretically, meaning the actual nonluminous behavior may be affected by other factors. Actually, the relaxation of molecular conformation is considered as an important reason affecting the radiation transition in many organic luminescent molecular systems [45]. Hence, we further compared and analyzed the optimized structures of B1-A1 in S_0 and S_1 state. For the sake of illustration, the dihedral angles of adjacent benzene rings in enamine chain were defined as α_1 and α_2 . As shown in Figure S14, α_1 and α_2 of B1-A1 were stated as 67.2° and 70.5° in S_0 state, as well as 52.1° and 55.0° in S_1 state, respectively. These results indicated the aggregating conformation of B1-A1 in S_1 excited state is prone to be

more planar than that in the ground state. This relaxation process partly consumes energy to promote non-radiative transitions, and the planar structures tend to format π - π interactions while aggregating. According to the RIM mechanism, these factors are unfavorable to the luminescence of B1-A1 in aggregation state, thus causing AIE/AIEE inactive effect.

In the same manner, theoretical calculation was employed to gain underlying awareness of the relationship between molecular structure and emission property on these substituted enamine derivatives. All derivatives exhibited distorted molecular conformations either in the ground state or the excited state, which contributed to the AIEE feature. In contrast to initial tetraphenyl enamine, the degree of relaxation and planarization from S_0 and S_1 state in all modified enamines became smaller (Table S3), revealing the reduction of non-radiative transition channels and the increased possibilities of the conversions from non-luminescence to AIEE active performance. Moreover, the conformational change degree is different in various compounds, thus causing their diverse AIEE behaviors. From these analysis results, we can infer that the introduced substituents solidify the conformations of these enamine derivatives, subsequently reducing their non-radiative energy consumption in aggregating state.

In the meantime, to deeply understand substituent tunable properties of all enamine compounds, their energy levels and electron cloud distributions of the HOMO and LUMO were simulated at the B3LYP/6-31G(d) level (Figure 5) [46]. Except NO_2 -B1-A1, the electronic densities of enamine derivatives in both the HOMO and LUMO levels are equally distributed, displaying that fully effective conjugations have been realized in short-length enamine chains and their structures are much rigid. The calculation also revealed that the energy levels and gaps could be modestly tuned by modifications with different electron donor abilities. From bromine to double methoxyls, the energy levels of the HOMOs (-4.97 to -4.54 eV) and LUMOs (-0.96 to -0.67 eV) in these four enamines gradually increased, con-

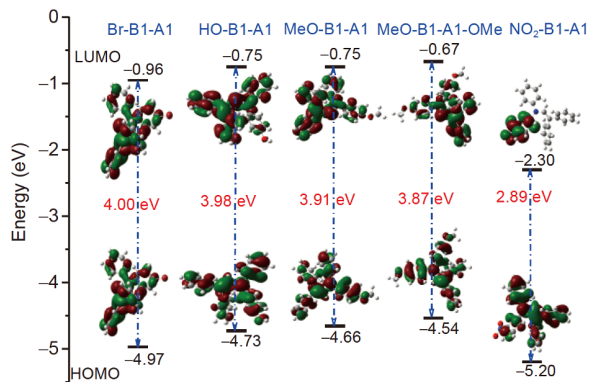


Figure 5 Energy levels and electron cloud distributions of the HOMO and LUMO of all enamine derivatives calculated at the B3LYP/6-31G(d) level by the DFT approach (color online).

forming to the respective electron donating effect of substituted groups. On account of the neutral feature of tetraphenyl enamine segment, the corresponding energy gaps of enamines are tightly affected by their modifications. Consequentially, as for the energy gaps between the HOMOs and LUMOs, the values for enamine derivatives lie in the range from 4.00 to 3.87 eV, with the smallest for MeO-B1-A1-OMe (3.87 eV) and the largest for Br-B1-A1 (4.00 eV), showing the agreement with their experimental spectral results. For NO₂-B1-A1, the electron cloud distributions of the HOMO and LUMO are separated owing to the distinct ICT effect. The HOMO is distributed on the whole molecule and mainly centered at the tetraphenyl enamine unit, while the LUMO mainly localizes on the nitrobenzene part. The strong electron-withdrawing nitro group tremendously reduces the energy levels in HOMO and LUMO, and a minor energy gap value generates to present near infrared luminescence [47].

3.5 Single-crystal structural analysis

To reveal their AIEE mechanism and emission feature, the single crystal analyses of all enamine derivatives are valuable. Analyzable single crystals of these compounds were able to be obtained through slow evaporation of CH₂Cl₂-hexane mixtures under mild conditions. As twin crystal is contained, it is specially noting that the single crystal structure of HO-B1-A1 is just used for studying intramolecular structural characteristics. The crystallographic data can be obtained free of charge from the Cambridge Crystallographic Data Centre with serial number CCDC 1994588, 2013819, 1994591, 1994592 and 1994595 for Br-B1-A1, HO-B1-A1, MeO-B1-A1, MeO-B1-A1-OMe and NO₂-B1-A1, respectively.

As shown in Figure S15, these enamine crystals all exhibit distorted molecular conformations with the dihedral angles of adjacent benzene ring exceeding 60°, which can effectively restrain the free rotations of phenyl and diphenyl en-

amine segments in aggregation. As well, in contrast to the computational data in ground state (Table S4), their relevant angle parameters (α_1 , α_2) mostly increase in the crystal state, which is beneficial to inhibit harmful interactions and promote AIEE effect. Notably, the degrees of distortion in these molecules are diverse, further affecting their different optical performance [48]. The dihedral angles of MeO-B1-A1-OMe are minimum in all auxochrome substituted enamines, thus showing higher planarity to produce longer absorption band. The similar trend also emerged in the solid emission peaks. Interestingly, the electronic and spatial effects sometimes work in opposite directions. A flatter conformation of HO-B1-A1 compound appears than MeO-B1-A1 molecule, while the auxochrome effect of methoxy is a bit stronger than hydroxyl. As a result, combining the corresponding electronic and configurable effects, HO-B1-A1 and MeO-B1-A1 reveal similar emission wavelength in both solution state and solid state.

The detailed packing structures of Br-B1-A1, MeO-B1-A1, MeO-B1-A1-OMe and NO₂-B1-A1 are given in Figure 6. Unlike common AIE/AIEE substances with parallel-slipped crystal stack, four compounds all exhibit loose molecular arrangements to hamper planar intermolecular interactions, which are put down to the high congestion resulting from the twisted structures. More importantly, multiple intermolecular interactions exist in these enamines. On one hand, these weak forces further assist in restraining molecular motion, which reduces the non-radiative deactivation of excitons and contributes to the conversion from non-luminescence to AIEE active performance. On the other hand, the

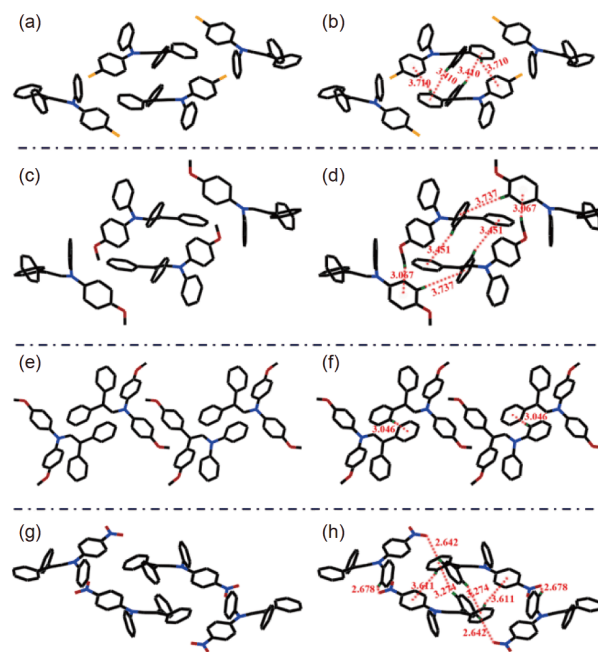


Figure 6 The packing patterns and intermolecular interactions of Br-B1-A1 (a, b), MeO-B1-A1 (c, d), MeO-B1-A1-OMe (e, f) and NO₂-B1-A1 (g, h), respectively. Hydrogen omitted for clarity (a, c, e, g) (color online).

intermolecular forces with various distances and strengths greatly affect the aggregated luminescence behaviors of these amine derivatives, causing their diverse AIEE behaviors. In view of Br-B1-A1 and MeO-B1-A1-OMe, only C–H \cdots π interactions between neighboring enamine derivative molecules were observed. Detailly, for Br-B1-A1 molecule, some C–H \cdots π hydrogen bonds with lengths of 3.4–3.7 Å are formed between the benzene rings in aniline monomer and stilbene. As for MeO-B1-A1-OMe, C–H \cdots π interactions with fixed bond length at 3.046 Å only exist in the adjacent stilbene moieties. These C–H \cdots π interactions are relatively limited and weak, thus leading to the smaller enhancement of fluorescence intensities when aggregating. On the contrary, the numbers of intermolecular interactions obviously improve in consideration of MeO-B1-A1 and NO₂-B1-A1, and the modified sections are found to participate in their intermolecular interactions at the same time. As for MeO-B1-A1, apart from C–H \cdots π hydrogen bonds in benzene units with lengths of 3.4–4.1 Å, the C–H \cdots π interactions between methoxyl and neighboring aniline parts are also discovered with a length of 3.067 Å. For NO₂-B1-A1, the distances of C–H \cdots π hydrogen bonds range from 3.2 to 3.6 Å, while the distances of NO₂ \cdots H interactions are just 2.646 Å. As we can see, these intermolecular interactions involving substituent groups are relatively strong to reduce nonradiative transitions by solidifying the structures of corresponding molecules, thus leading to higher enhancement ratios of luminous intensities from monomolecular state to aggregating state [49]. Therefore, AIEE properties of these enamines may be tuned by selecting specific substituents through regulating and controlling relevant intermolecular forces, which further provide a constructive method of building more AIE/AIEE systems with p- π conjugate chain structures.

4 Conclusions

In summary, based on a novel p- π conjugate chain structure (–C=C–N–), a series of tetraphenyl enamine cored derivatives with various terminal groups have been designed and synthesized. The photo-physical investigation showed that these compounds all exhibited AIEE behaviors, meaning the successful conversion from non-luminance to AIEE-activity of tetraphenyl enamine could be achieved by rational modifications. Moreover, the emission performance of enamines could be effectively adjusted by various side groups, revealing substituent tunable emission properties. In comparison to their pure THF solution, the luminous intensities of HO-B1-A1, MeO-B1-A1 and NO₂-B1-A1 solutions containing 95% water increased by more than 90 times, whereas enhancement ratios of Br-B1-A1 and MeO-B1-A1-OMe were below 10-fold. As well, the luminescence wavelength and solid fluorescence of the enamine derivatives were able

to be effectually regulated by diverse substituents. In virtue of theoretical calculation and single crystal investigation, we concluded that the introduced side groups readily increased the degree of conformation distortion and provided multiple intermolecular interactions to solidify molecular structures, which promoted radiative decay rate and block nonradiative channel *via* the restriction of intramolecular rotation (RIR) mechanism. In particular, the participation of the modified sections in intermolecular interactions can dramatically improve AIEE effect of the corresponding enamines. These results not only contribute to the understanding of the enamines' substituent influence on photo-physical properties, AIEE properties, electronic structure and molecular packing, but also offer basic knowledge for further functional modification of other kinds of AIE/AIEE units to obtain new AIE/AIEE materials.

Acknowledgements This work was supported by the National Natural Science Foundation of China (21574003).

Conflict of interest The authors declare no conflict of interest.

Supporting information The supporting information is available online at <http://chem.scichina.com> and <http://link.springer.com/journal/11426>. The supporting materials are published as submitted, without typesetting or editing. The responsibility for scientific accuracy and content remains entirely with the authors.

- 1 Chen Y, Lam JWY, Kwok RTK, Liu B, Tang BZ. *Mater Horiz*, 2019, 6: 428–433
- 2 Gao M, Tang BZ. *ACS Sens*, 2017, 2: 1382–1399
- 3 La DD, Bhosale SV, Jones LA, Bhosale SV. *ACS Appl Mater Interfaces*, 2018, 10: 12189–12216
- 4 Mei J, Huang Y, Tian H. *ACS Appl Mater Interfaces*, 2018, 10: 12217–12261
- 5 Feng G, Liu B. *Acc Chem Res*, 2018, 51: 1404–1414
- 6 Yan L, Zhang Y, Xu B, Tian W. *Nanoscale*, 2016, 8: 2471–2487
- 7 Liu B, Nie H, Zhou X, Hu S, Luo D, Gao D, Zou J, Xu M, Wang L, Zhao Z, Qin A, Peng J, Ning H, Cao Y, Tang BZ. *Adv Funct Mater*, 2016, 26: 776–783
- 8 Guo J, Li XL, Nie H, Luo W, Hu R, Qin A, Zhao Z, Su SJ, Tang BZ. *Chem Mater*, 2017, 29: 3623–3631
- 9 Yang J, Chi Z, Zhu W, Tang BZ, Li Z. *Sci China Chem*, 2019, 62: 1090–1098
- 10 Sasaki S, Suzuki S, Sameera WMC, Igawa K, Morokuma K, Konishi G. *J Am Chem Soc*, 2016, 138: 8194–8206
- 11 Tu Y, Liu J, Zhang H, Peng Q, Lam JWY, Tang BZ. *Angew Chem Int Ed*, 2019, 58: 14911–14914
- 12 Zhang H, Zhao Z, McGonigal PR, Ye R, Liu S, Lam JWY, Kwok RTK, Yuan WZ, Xie J, Rogach AL, Tang BZ. *Mater Today*, 2020, 32: 275–292
- 13 Leung NLC, Xie N, Yuan W, Liu Y, Wu Q, Peng Q, Miao Q, Lam JWY, Tang BZ. *Chem Eur J*, 2014, 20: 15349–15353
- 14 Islam MM, Hu Z, Wang Q, Redshaw C, Feng X. *Mater Chem Front*, 2019, 3: 762–781
- 15 Meher N, Panda S, Kumar S, Iyer PK. *Chem Sci*, 2018, 9: 3978–3985
- 16 Yang Z, Chi Z, Mao Z, Zhang Y, Liu S, Zhao J, Aldred MP, Chi Z. *Mater Chem Front*, 2018, 2: 861–890
- 17 Viglianti L, Leung NLC, Xie N, Gu X, Sung HHY, Miao Q, Williams ID, Licandro E, Tang BZ. *Chem Sci*, 2017, 8: 2629–2639
- 18 Wang ZL, Ma K, Xu B, Li X, Tian WJ. *Sci China Chem*, 2013, 56:

- 1234–1238
- 19 Jana R, Pathak TP, Sigman MS. *Chem Rev*, 2011, 111: 1417–1492
- 20 Akbari A, Arsalani N, Amini M, Jabbari E. *J Mol Catal A-Chem*, 2016, 414: 47–54
- 21 Wang Y, Pan X, Peng Z, Zhang Y, Liu P, Cai Z, Tong B, Shi J, Dong Y. *Sens Actuatur B-Chem*, 2018, 267: 351–356
- 22 Zhang Y, Mao H, Xu W, Shi J, Cai Z, Tong B, Dong Y. *Chem Eur J*, 2018, 24: 15965–15977
- 23 Hou J, Du J, Hou Y, Shi P, Liu Y, Duan Y, Han T. *Spectrochim Acta Part A-Mol Biomol Spectr*, 2018, 205: 1–11
- 24 Sun J, Yuan J, Li Y, Duan Y, Li Z, Du J, Han T. *Sens Actuatur B-Chem*, 2018, 263: 208–217
- 25 Sairi AS, Kuwahara K, Sasaki S, Suzuki S, Igawa K, Tokita M, Ando S, Morokuma K, Suenobu T, Konishi G. *RSC Adv*, 2019, 9: 21733–21740
- 26 Liu D, Li J, Liu J, Lu X, Hu M, Li Y, Shu Z, Ni Z, Ding S, Jiang L, Zhen Y, Zhang X, Dong H, Hu W. *J Mater Chem C*, 2018, 6: 3856–3860
- 27 Mon M, Ferrando-Soria J, Grancha T, Fortea-Pérez FR, Gascon J, Leyva-Pérez A, Armentano D, Pardo E. *J Am Chem Soc*, 2016, 138: 7864–7867
- 28 Segura JL, Mancheño MJ, Zamora F. *Chem Soc Rev*, 2016, 45: 5635–5671
- 29 Saito M, Shinokubo H, Sakurai H. *Mater Chem Front*, 2018, 2: 635–661
- 30 Chang Y, Yesilcimen A, Cao M, Zhang Y, Zhang B, Chan JZ, Wasa M. *J Am Chem Soc*, 2019, 141: 14570–14575
- 31 Zhu L, Zhang L, Luo S. *Angew Chem Int Ed*, 2018, 57: 2253–2258
- 32 Wang Z, Tian C, Liu Q, Zhang W, Pan C, Su G. *Chin J Org Chem*, 2019, 39: 1962–1969
- 33 Lu H, Wang K, Liu B, Wang M, Huang M, Zhang Y, Yang J. *Mater Chem Front*, 2019, 3: 331–338
- 34 Li W, Cai X, Li B, Gan L, He Y, Liu K, Chen D, Wu Y, Su S. *Angew Chem Int Ed*, 2019, 58: 582–586
- 35 Sun H, Tang XX, Zhang R, Sun WH, Miao BX, Zhao Y, Ni ZH. *Dyes Pigments*, 2020, 174: 108051
- 36 Huang W, Tang F, Li B, Su J, Tian H. *J Mater Chem C*, 2014, 2: 1141–1148
- 37 Liu S, Cheng J, Xu J. *Chin J Chem*, 2017, 35: 335–340
- 38 Amendola V, Meneghetti M. *J Phys Chem C*, 2009, 113: 4277–4285
- 39 Zhang Y, Wang JH, Zheng J, Li D. *Chem Commun*, 2015, 51: 6350–6353
- 40 Zhao W, He Z, Peng Q, Lam JWY, Ma H, Qiu Z, Chen Y, Zhao Z, Shuai Z, Dong Y, Tang BZ. *Nat Commun*, 2018, 9: 3044–3051
- 41 Nie H, Hu K, Cai Y, Peng Q, Zhao Z, Hu R, Chen J, Su SJ, Qin A, Tang BZ. *Mater Chem Front*, 2017, 1: 1125–1129
- 42 Xu Z, Gu J, Qiao X, Qin A, Tang BZ, Ma D. *ACS Photon*, 2019, 6: 767–778
- 43 Zhang H, Nie Y, Miao J, Zhang D, Li Y, Liu G, Sun G, Jiang X. *J Mater Chem C*, 2019, 7: 3306–3314
- 44 Chen M, Hu X, Liu J, Li B, Leung NLC, Viglianti L, Cheung TS, Sung HHY, Kwok RTK, Williams ID, Qin A, Lam JWY, Tang BZ. *Chem Sci*, 2018, 9: 7829–7834
- 45 Tanaka K, Nishino K, Ito S, Yamane H, Suenaga K, Hashimoto K, Chujo Y. *Faraday Discuss*, 2017, 196: 31–42
- 46 Xu B, Li W, He J, Wu S, Zhu Q, Yang Z, Wu YC, Zhang Y, Jin C, Lu PY, Chi Z, Liu S, Xu J, Bryce MR. *Chem Sci*, 2016, 7: 5307–5312
- 47 Fu W, Yan C, Guo Z, Zhang J, Zhang H, Tian H, Zhu WH. *J Am Chem Soc*, 2019, 141: 3171–3177
- 48 Peng Z, Ji Y, Huang Z, Tong B, Shi J, Dong Y. *Mater Chem Front*, 2018, 2: 1175–1183
- 49 Yin X, Fan JZ, Liu J, Cai L, Sun H, Sun YP, Wang CK, Lin LL. *Phys Chem Chem Phys*, 2019, 21: 7288–7297